13th World Conference on Earthquake Engineering
Vancouver, B.C., Canada
August 1-6, 2004
Paper No. 1884

APPLICATION OF SMA RODS TO EXPOSED-TYPE COLUMN BASES IN SMART STRUCTURAL SYSTEMS

Hiroyuki TAMAI [1], Yoshikazu KITAGAWA [2] and Toshibumi FUKUTA [3]

SUMMARY

A seismic-resistant member with a shape memory alloy (SMA) rod was used in an exposed-type column base as a passive damper for building structures. Horizontal and vertical loading tests on the column base with SMA anchorage were done with increasing drift amplitude to investigate the restoring force characteristics of the column base. Also, a numerical model of a column base with SMA anchorage was derived, and simulations of this column base under cyclic loading were then performed. Both the experimental and numerical results showed that (1) use of an SMA rod prevents deterioration of the restoring force characteristics, (2) use of an appropriate SMA material and a moderate-size rod can yield large deformation capacity and good restoring force characteristics, and (3) after a large drift in the building frame, SMA anchorage enables the column base to recover to its original shape and resistance performance after unloading.

INTRODUCTION

In recent years, the unique properties of shape memory alloys (SMA) have attracted the attention of many researchers for application to smart structural systems. These properties are shape memory effect and pseudoelastic effect.

At a certain temperature, an SMA rod is stretched to apparent yield so that residual strain remains. Then, heating to a particular temperature causes the residual strain to disappear. This phenomenon is called shape memory effect (SME). Heating to a different particular temperature causes the strain to fully recover with unloading. This phenomenon is called pseudoelastic effect (PE). Both SME and PE are caused by phase transformation [1]. Despite the development of SME-PE-based actuators and dampers used in civil and aerospace structures [2-4], passive hysteretic dampers for severe earthquakes are still used in building structures [5]. SMA rod designed for seismic-resistant members of building structures has been developed by Daido Steel Co. Ltd. The material properties of this SMA wire have been reported [6], and revealed that (1) an SMA rod recovers its original shape with unloading after 5% axial elongation, and absorbs energy effectively by means of its pseudoelastic deformation, (2) use of an SMA member as a

[1] Associate Professor, Faculty of Engineering, Hiroshima Institute of Technology, Dr. of Eng., tamrix@cc.it-hiroshima.ac.jp
[2] Professor, Faculty of Science and Technology, Keio University, Dr. of Eng., kitagawa@sd.keio.ac.jp
[3] Manager, Building Research Institute, Dr. of Eng., fukuta@kenken.go.jp

building structural member subjected to large deformation might improve the deformation capacity and improve the repair performance of a building structural system needed after an earthquake.

In this study, we developed a seismic-resistant member that contains an SMA rod incorporated in an exposed-type column base as a passive damper in building structures. To investigate the mechanical properties of this exposed-type column base, vertical and horizontal loading tests were done using a cantilever. Then, a numerical model of a column base with SMA anchorage was developed and used to simulate this column base under cyclic loading. Both the experimental and simulation results showed that the applicability and availability of the SMA rod for seismic-resistant members.

APPLICATION OF SMA WIRE TO BUILDING STRUCTURES

As discussed above, the pseudoelastic effect of SMA enables a member to recover its original shape. Furthermore, due to its pseudoelastic deformation, SMA effectively absorbs the energy inputted. One particular SMA, nitinol, has high strength (about 850 MPa) and stiffness (about 40 GPa) compared with steel, and thus is easily applied to seismic-resistant members of practical dimensions. Furthermore, large-diameter SMA wire (approximately 20-30 mm in diameter) can be produced by Daido Steel Co. Ltd. Thus, in this study, this large-diameter SMA wire was applied to seismic-resistant members of building structures as follows.

Exposed-type column base with SMA anchorage

Figure 1 shows the developed SMA anchorage, where a column was welded to a steel base plate. The base plate was fastened to the base with anchor bolts. Each anchor bolt consisted of an SMA rod connected to an ordinary steel bolt via a coupler. A sheath enclosed each SMA bolt to enable repair after an earthquake. The maximum strength of the SMA bolts was set smaller than that of the steel bolts, the end of the column, and the base plate.

In this structural system, in accordance with seismic design demands, the initial elastic limit displacement and strength were adjustable by changing the length and cross-sectional area of the steel bolt and the cross-sectional area of the SMA rod. In an SMA rod, restoring force characteristics do not degrade and the seismic energy inputted to the structural frame is absorbed effectively due to the rod's pseudoelastic deformation. Furthermore, large deformation capacity can be expected without column yielding. Therefore, reducing the responses of a building frame to prevent serious damage to the frame under a severe earthquake is possible, and repair of the frame is easily accomplished by simply replacing the SMA members after the earthquake.

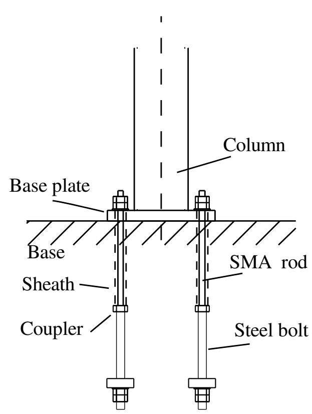

Figure 1: Application of SMA rod to building structure with exposed-type column base with SMA anchorage.

NUMERICAL MODEL OF SMA ROD

A numerical model of the restoring force of SMA is indispensable in simulating the performance of the seismic-resistant members under seismic working load. Based on previous experimental results [6], a phenomenological model with an internal variable of SMA [1-3] is introduced here from an engineering point of view. This model was used to verify the measured behavior of the SMA rod [6].

Facts and assumptions used in the numerical model

The well-known properties and phase transformation of nitinol are as follows [1]:

1) Martensitic transformation (forward transformation) is non-diffusive. That is, development of transformation is defined by the total state variables independently of time.
2) Thermal expansion coefficient of nitinol is around 6-11 x 10^{-6} K^{-1}. Therefore, the thermal strain in the material is negligible when the material temperature is less than 100 K.

From the test results [6], the following assumptions were used in this model:

1) Only the austenite and martensite phases are considered, because the effects of rhombohedral phase transformation are negligible.
2) Transformations strongly depend on temperature and stress. The stress-induced transformation lines are assumed linear.

For simplicity, the following assumptions were also used in the model.

1) Residual strain (e.g. plasticity) under cyclic loading is ignored.
2) Although elastic modulus E and transformation coefficient Ω are dependent on the material temperature T and the volume fraction of martensite ξ in general, E and Ω are assumed constant.
3) The temperature field in the material is given beforehand. Heat conduction and transmission analysis are outside the scope of this paper.

Based on these facts and assumptions, thermomechanical constitutive relations in the model are derived as follows:

$$\dot{\varepsilon} = \dot{\varepsilon}_e + \dot{\varepsilon}_t \tag{1.a}$$

$$\dot{\sigma} = E \cdot \dot{\varepsilon} + \Omega \cdot \dot{\xi} \tag{1.b}$$

$$\xi = \xi(\sigma, T) \tag{1.c}$$

where σ is cauchy stress, $\dot{\varepsilon}$ is total strain velocity, $\dot{\varepsilon}_e$ is elastic strain velocity, $\dot{\varepsilon}_t$ is transformation strain velocity, ξ and $\dot{\xi}$ is volume fraction of martensite ($0 < \xi < 1$) and its velocity, respectively. From the definition of elastic strain and Eqs.(1.a), (1.b), following relations are derived.

$$\dot{\varepsilon}_e = E^{-1} \cdot \dot{\sigma} \tag{2.a}$$

$$\dot{\varepsilon}_t = -E^{-1} \cdot \Omega \cdot \dot{\xi} \tag{2.b}$$

The kinetics of stress-induced transformations under uniaxial stress state are assumed as follows.
For forward transformation,

$$\xi = \xi(\sigma, T) = a_M \cdot (M_s - T) + b_M \cdot \sigma \tag{3.a}$$

For reverse transformation,

$$\xi = \xi(\sigma, T) = 1 - \langle a_A \cdot (A_s - T) + b_A \cdot \sigma \rangle \tag{3.b}$$

where Ms, As are the martensite and austenite initial temperatures under zero external stress, and a_M, b_M, a_A and b_A are parameters derived from experimental data. Note that ξ varies from 0 to 1. Because ξ increases under developing martensite transformation and decreases under developing reverse transformation, the development conditions of transformations are derived as follows.

For forward transformation,

$$-a_M \cdot \dot{T} + b_M \cdot \dot{\sigma} \geq 0 \qquad \text{for} \quad a_M \cdot (M_s - T) + b_M \cdot \sigma \geq 0 \tag{4.a}$$

For reverse transformation,

$$-a_A \cdot \dot{T} + b_A \cdot \dot{\sigma} \geq 0 \qquad \text{for} \quad a_A \cdot (A_s - T) + b_A \cdot \sigma \geq 0 \tag{4.b}$$

The values ξ=1.0 and ξ=0.0 indicate completed forward and reverse transformations, respectively. Considering the following conditions for ξ, T, and σ, the parameters a_M, b_M, a_A, and b_A given by Eqs.(3.a),(3.b) can be expressed as follows.

$$\xi = 1.0 \quad \text{for} \quad T = M_s, \quad \sigma = \Delta\sigma_M \qquad \xi = 1.0 \quad \text{for} \quad T = M_f, \quad \sigma = 0.0$$

$$\xi = 0.0 \quad \text{for} \quad T = A_s, \quad \sigma = \Delta\sigma_A \qquad \xi = 0.0 \quad \text{for} \quad T = A_f, \quad \sigma = 0.0$$

$$a_M = -\frac{1}{M_f - M_s}, \quad b_M = \frac{1}{\Delta\sigma_M} \tag{5.a,b}$$

$$a_A = -\frac{1}{A_f - A_s}, \quad b_A = \frac{1}{\Delta\sigma_A} \tag{5.c,d}$$

where M_f, A_f are the martensite and austenite final temperatures under zero external stress, and $\Delta\sigma_M$, $\Delta\sigma_A$ are isothermal stress widths from initial to final transformation (see Figs. 2a,b).

Let us now consider the unloading process, when martensite transformation has not finished. Assuming that contribution of reverse transformation to ξ depends on the volume fraction of martensite ξ_R at unloading, then kinetics of reverse transformation is written as follows.

$$\xi = \xi(\sigma, T) = \xi_R \cdot \left\{1 - \left\langle a_A \cdot (A_s - T) + b_A \cdot \sigma \right\rangle\right\} \tag{6}$$

Also, integrating Eq.(1.b) from ξ=0 to a certain time ξ=1 yields

$$\Omega = \sigma_{Mf} - E \cdot \varepsilon_{Mf} \tag{7}$$

where ε_{Mf}, σ_{Mf} are the increment in strain and stress, respectively, from ξ=0 to ξ=1 under monotonic loading.

The thermomechanical material constants of the SMA rods were derived from the experimental data from monotonic loading and pulsating tension loading tests [6,7]. The calculated constants of two different SMA materials (denoted as A and B) are shown in Table 1. Figures 2(a,b) show assumed transformational kinetics lines and phase transform stress vs. ambient temperature T_a based on experimental results [6,7]. When T and σ are given, ξ_R for martensite can be derived from Eqs.(3.a),(3.b). Then, the increment in transformation strain, the elastic strain and the total strain are derived from Eqs.(2.b), (2.a), (1.a), respectively. The hysteresis loop for the SMA rod is obtained by repeating the above procedures judging the stop and development of the transformation from Eqs.(4.a), (4.b).

Verification of the numerical model of the column base with SMA anchorage

To verify the validity and accuracy of the numerical model column base with SMA anchorage, predictions of σ vs. ε relation by using this model were compared with experimental results [6,7]. Two sets of conditions were used: a pulsating tension loading at strain amplitude ε_{max} =3% under ambient temperature

T_a=288K, 298K, 308K, 318K (15°C, 25 °C, 35 °C, 45 °C), and a pulsating tension loading at ε_{max} =5% under T_a =280 K, 283 K, 293 K, 308 K (7°C, 10°C, 20 °C, 35 °C). These two cases were based on the assumption that $T = T_a$. Figures 3(a,b) show the measured and simulated σ and ε.
The results yielded the following conclusions.

i) The model can reproduce the spindle-shaped hysteresis loop for a SMA rod without residual deformation and stress, which the initial phase transformation stress is sensitive to T_a.
ii) The model can quantitatively predict the pseudoelastic behavior of nitinol at various T_a.

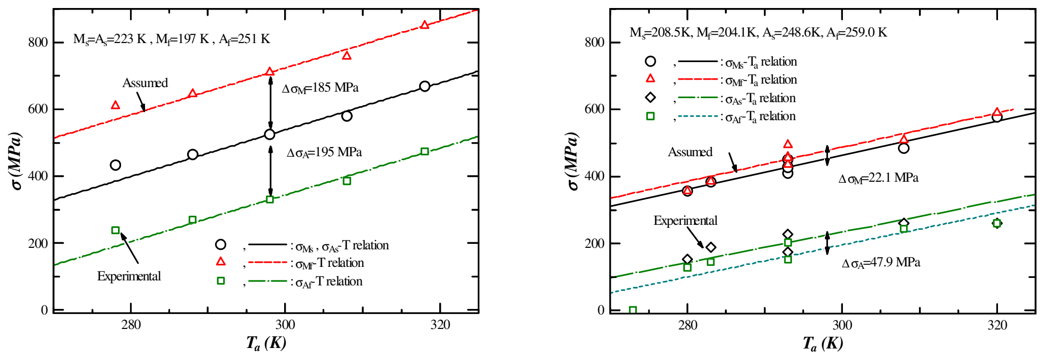

(a) SMA of Material A (10.0mm diameter). (b) SMA of Material B (1.7mm diameter)

Figure 2(a), (b): Phase transform stress σ vs. ambient temperature T_a.

Table 1: Thermomechanical properties of SMA rods.

SMA Material Properties	M_s	M_f	A_s	A_f	$\Delta\sigma_M$	$\Delta\sigma_A$	Ω
	K	K	K	K	MPa	MPa	MPa
A	223	196.5	223	250.9	185	195	-8.9x10^2
B	204.1	208.5	248.6	259	22.1	47.9	-1.6x10^3

M_s, M_f, A_s, A_f Transformation temperature.
$\Delta\sigma_A$, $\Delta\sigma_M$ Transformation transit stress width.
Ω Coefficient of transformational kinetics.

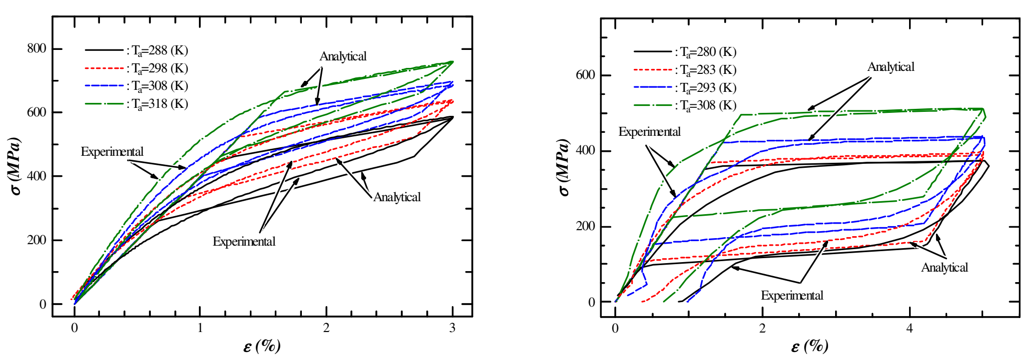

(a) SMA of material A (10.0mm diameter) (b) SMA of material B (1.7mm diameter)

Figure 3(a), (b): Experimental and simulated stress σ vs. strain ε

LOADING TESTS OF COLUMN BASE

To clarify the resistance mechanism in column base with SMA anchorage, vertical and horizontal loading tests were done using a cantilever with SMA anchorage. For comparison, the same tests were done using a cantilever with anchorage typically used in current construction.

Test specimen and loading program

Figures 4 and 5 show the test apparatus and specimens, respectively. The specimens were cantilevers with an exposed-type column base fastened by SMA anchor bolts or typical (SS400) anchor bolts. Each SMA anchor bolt consisted of two screw joints and an SMA rod (Fig. 6). The SMA rod was made of Ti-54.41wt%-Co and heat-treated in a furnace at 673K(400^{o}C) for 1h, then quenched with water. The rod, designed by Daido Steel Co. Ltd., showed pseudoelastic effect at room temperature. Each typical anchor bolt was made of SS400 steel. Table 1 lists the thermomechanical properties of SMA rod made of material A, and Table 2 lists the mechanical properties of the specimens.

The loading program (Fig. 7) was pulsating horizontal loading with constant axial force. From the upper stub, an axial force, N, and a prescribed horizontal displacement, δ_h, were applied to the specimen (Fig. 9) for various number of cycles, n (Fig. 7). Each cycle was a constant N = 196kN, with horizontal pulsating loading at incremental intensity of δ_h =10.0mm, 15.0mm, 20.0mm, 25.0mm. During the tests, T_a was kept at 295K (22^{o}C).

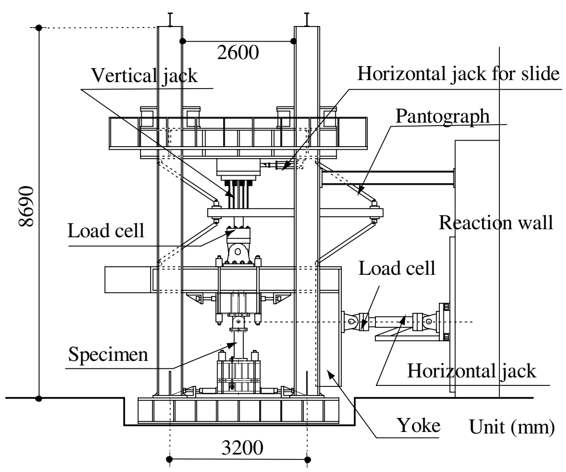

Figure 4: Test apparatus.

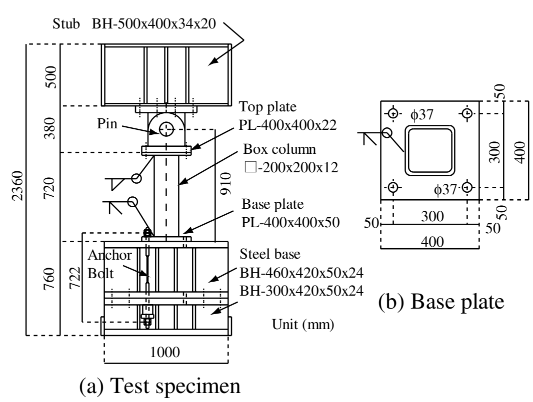

Figure 5: Test specimen.

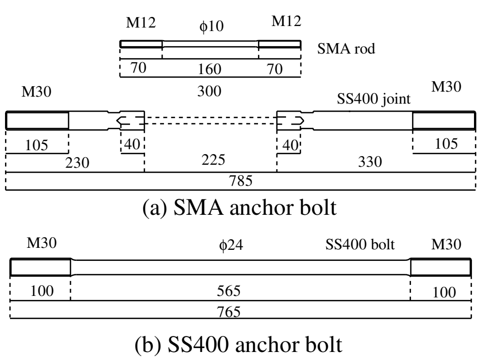

Figure 6: SMA and typical (SS400) anchor bolts.

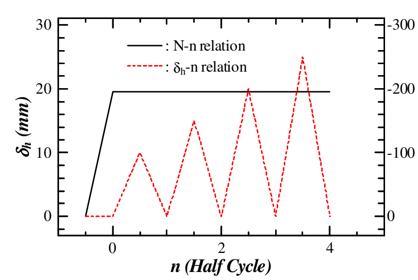

Figure 7: Loading programs.

Measurement and evaluation of reaction force

Figure 9 shows the instruments used to measure the horizontal and vertical displacements at the loading point (δ_h and δ_v, respectively), the relative rotational angle between the base plate and base (θ_r), the relative vertical displacement between the base plate and base (w_r), and the averaged strain of the anchor bolt in a smaller section (ε). In each test, θ_r was obtained as the slope calculated from the vertical displacements of the left and right edges of the base plate, ε was measured by an extensometer with an initial gauge length of 50mm, and δ_h, δ_v, and w_r were obtained as the average of measured values from the front and rear transducers. All transducers, except the extensometer, were supported by instruments fixed at the center of the steel base.

Loading measurements included the axial force (N), the bending moment (M), the shear force at the lower end of the column (Q), and the tensile force of each anchor bolt (P). In the tests, N, M, and Q were obtained from load cells at the top of vertical and horizontal jacks, and P was obtained from load cells attached at the lower end of the anchor bolts.

Equilibrium conditions of the test specimen (Fig. 8) were expressed as follows.

$$N + C = P \tag{8.a}$$

$$M + d_c \cdot N = (d_c + d_t) \cdot P \tag{8.b}$$

where C is the concentrated reaction force from the base, P is axial force of the tensile-side anchor bolts, and d_c and d_t are distance from the centroid of the column to the point of reaction force and that from the centroid to the tensile-side anchor bolt, respectively.

Because M, N, and P were measured directly, the two remaining variables, C and d_c, were derived from Eqs.(8.a.b) as follows

$$C = P - N \tag{9.a}$$

$$d_c = \frac{M - d_t \cdot P}{P - N} \tag{9.b}$$

From Eq.(8.b), M and Q were divided into the contribution of the axial force of the column (M_N, Q_N) and that of the axial force of the tensile-side anchor bolts (M_A, Q_A) as follows.

$$M = M_N + M_A \quad , \quad Q = Q_N + Q_A \tag{10.a,b}$$

where

$$M_N = -d_c \cdot N \quad , \quad Q_N = \frac{-d_c \cdot N}{L} \tag{11.a,b}$$

$$M_A = (d_c + d_t) \cdot P \quad , \quad Q_A = \frac{(d_c + d_t) \cdot P}{L} \tag{11.c,d}$$

where L is the length of the cantilever.

The standard values of δ_y, θ_y, and (M_y, Q_y) when the anchor bolts yielded under $N=0$ were used to normalize the test results for comparison. These values were derived based on the following assumptions: (1) d_c is the half-width of the column, (2) no elastic deformation occurs in the base plate and base, (3) column remains elastic, and (4) rotational center of the base plate is the flange edge of the column (Fig.8). Table 3 shows these standard values.

Table 2: Mechanical properties of materials.

Portion of material	Material	$E(GPa)$	$\sigma_y\ (MPa)$	$\sigma_u\ (MPa)$	$\varepsilon_{st}\,(\%)$	$\varepsilon_f\,(\%)$
Box column (□ -200x200x12)	STKR400	205.8	378.5	439.3	-	35.0
Base plate (PL-400x400x50)	SS400	205.8	260.9	413.8	1.30	37.0
SMA rod (Φ10)	Nitinol	40.0	524.0	850.0	-	5.2
SS400 bolt, joint (Φ 24,Φ30)	SS400	205.8	246.5	476.1	0.85	24.4

σ_y:Yield stress, Martensite start transformation stress , σ_u:Tensile strength,
E : Young's modulus, ε_{st} : Strain at hardening observed, ε_f : Elongation

Table 3: Standard values of responses.

	with SMA anchor	with SS400 anchor
$\delta_y\ (mm)$	11.9	4.49
$\theta_y\ (rad)$	0.0125	0.0033
$Q_y\ (kN)$	22.6	61.3
$M_y\ (MN \cdot mm)$	20.6	55.8

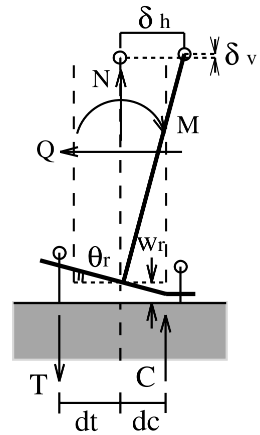

Figure 8: Schematic of column base.

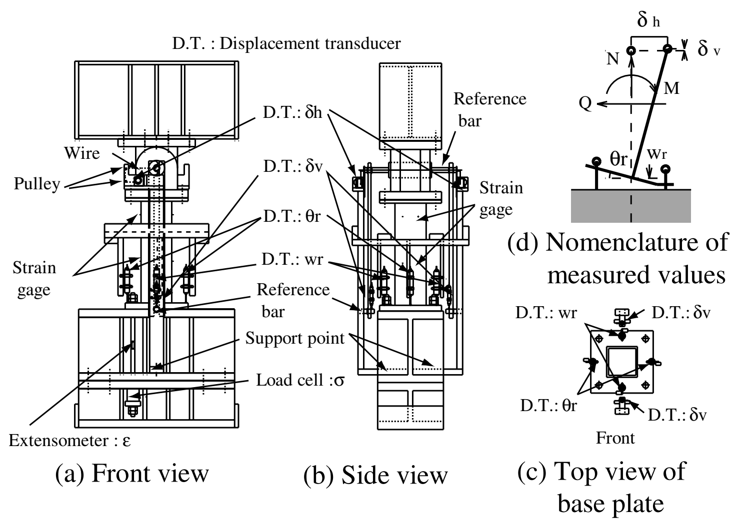

Figure 9: Measurement instruments and nomenclature.

EXPERIMENTAL RESULTS

The results from the loading the tests are shown in Figures 10-13 and Photographs 1-3. Figure 10 shows M vs. θ_r, d_c vs. θ_r, and σ vs. ε as a function of n for the column-base specimen with SMA anchorage, and Fig.11 shows those for the specimen with typical anchorage. Figure 12 shows Q_A/Q_y vs. δ_h/δ_y and M_A/M_y vs. θ_r/θ_y as a function of n for the column-base specimen with SMA anchorage, and Fig. 13 shows those for the specimen with typical anchorage. Photograph 1 shows the residual deformation of the two types of anchor bolts after the loading tests. Photograph 2 shows the bending deformation of the anchor bolts due to leverage of the base plate for the specimen with SMA anchorage.

After the loading test for the specimen with SMA anchorage, monotonic horizontal loading was done on the same specimen with the SMA anchorage until the SMA rod failed (θ_r =0.03rad, ε=2.5%). Photograph 3 shows the failure position and surface a-a' section of the SMA rod under this monotonic horizontal loading.

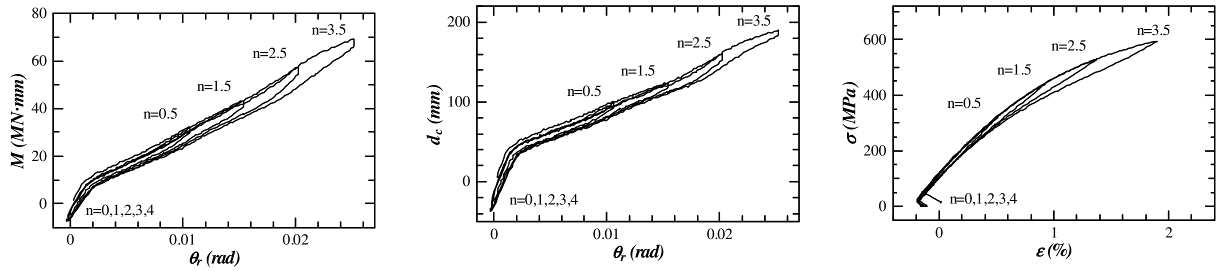

(a) M vs. θ_r. (b) d_c vs. θ_r. (c) σ vs. ε.

Figure 10: M vs. θ_r , d_c vs. θ_r and σ vs. ε for the column base with SMA anchorage.

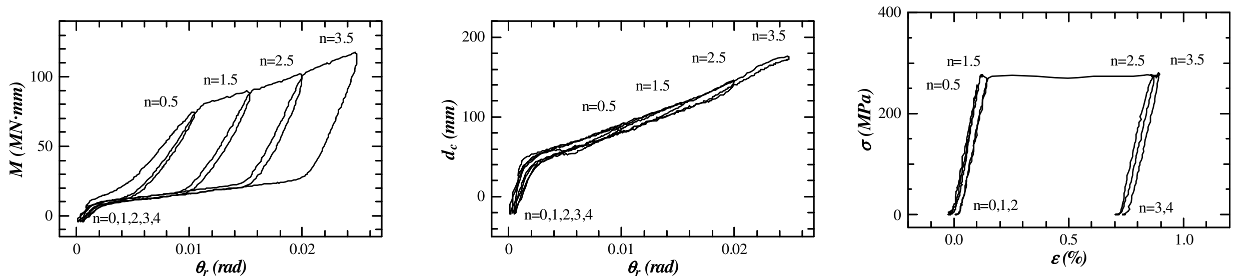

(a) M vs. θ_r. (b) d_c vs. θ_r. (c) σ vs. ε.

Figure 11: M vs. θ_r, d_c vs. θ_r, σ vs. ε for the column base with typical anchorage.

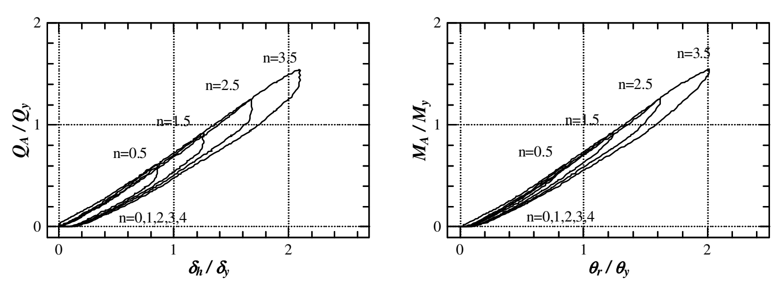

(a) Q_A/Q_y vs. δ_h/δ_y. (b) M_A / M_y vs. θ_r/θ_y.

Figure 12: Q_A/Q_y vs. δ_h/δ_y and M_A / M_y vs. θ_r/θ_y for the column base with SMA anchorage.

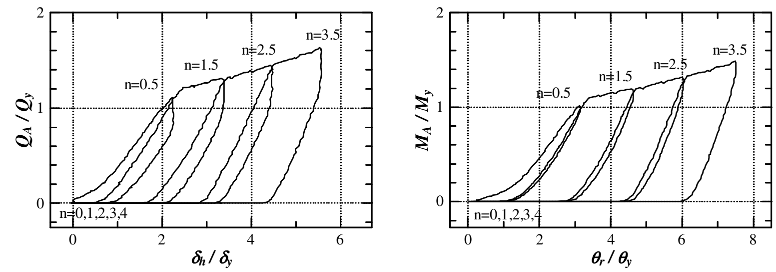

(a) Q_A/Q_y vs. δ_h/δ_y.　　(b) M_A / M_y vs. θ_r/θ_y .

Figure 13: Q_A/Q_y vs. δ_h/δ_y and M_A / M_y vs. θ_r/θ_y for the column base with typical anchorage.

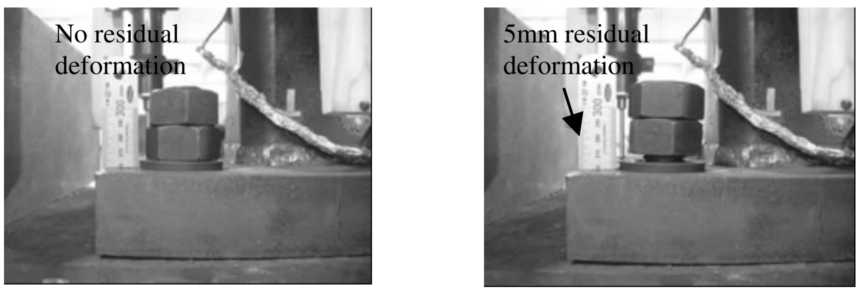

(a) SMA anchor bolt.　　(b) Typical (SS400) anchor bolt.

Photograph 1: Residual deformation of anchor bolts after loading test.

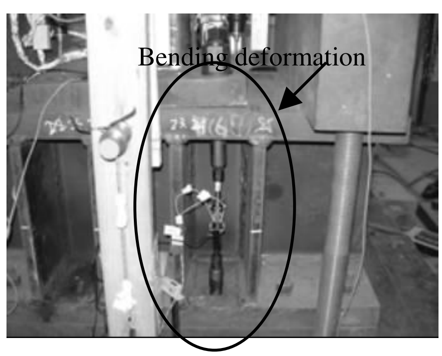

Photograph 2: Bending deformation for SMA anchor bolts due to leverage at 3.5 half-cycles.

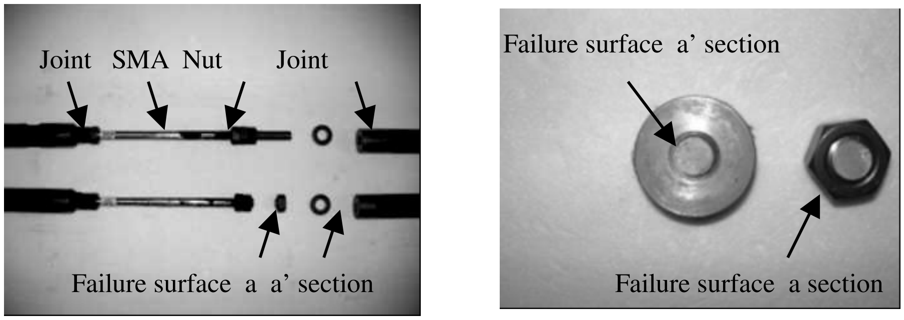

(a) Failure position. (b) Failure surface of SMA rod.

Photograph 3: Failure position and surface of an SMA rod.

These results can be summarized as follows.

i) Although M vs. θ_r relation showed a complicated hysteresis loop (Figs.10(a),11(a)), contribution of the anchor bolts and N to M can be evaluated using Eqs. (9.b) and (11.a,c).

ii) The d_c vs. θ_r relation could be expressed by bi-linear lines, and was independent of the restoring force characteristics of the anchor bolt (Figs.10(b),11(b)).

iii) In the specimen with typical anchorage, rotational stiffness in M_A/M_y vs. θ_r/θ_y was 30% of its initial rotational stiffness after the anchor bolt yielded (Fig.10(a)). Also, there was no resistance force until θ_r equaled the rotation when $M_A = 0$ in a previous loading cycle. In contrast, in the specimen with SMA anchorage, rotational stiffness was almost the same as its initial rotational stiffness when $(M_A/M_y) > 1.0$, and the (M_A/M_y) vs. (θ_r/θ_y) relation recovered to its original state under complete unloading.

iv) Rotational stiffness of the column base was considerably smaller than that when the base and base plate were assumed to be rigid (Figs.10(a),11(a)).

v) In the specimen with typical anchorage, the residual deformation accumulated in accordance with n (Fig.13(b)). The anchor bolt came out from the base. Therefore, there was slip in the restoring force characteristics, and the hysteresis loop deteriorated. In contrast, the SMA anchor bolts recovered both their original shape and their resistance performance after large repeated rotation of the base plate (Photo.1(a)). In the specimen with SMA anchorage, a large restoring force can be expected when $\theta < 0.025$rad.

vi) Leverage of the base plate caused the SMA anchor bolt to bend when δ_h was relatively large ($\delta_h > 5\delta_y$) (Photo.2). Due to bending deformation of the anchor bolt, brittle fracture occurred at the screw joint between the SMA rod and joint bolts.

vii) Fracture strain of the SMA rod in the loading test (ε=2.5%) was about half of that in the material test (ε=5.2%), suggesting that the bending deformation and the notch in the screw reduced the deformation capacity of the SMA rod.

When apparent yielding (phase transformation) occurred in the SMA anchor bolt and the SMA stiffness decreased compared with its initial stiffness (Fig.10(c)), the rotational stiffness of the column base did not decrease, which can be explained as follows. Increasing the rotation of the base plate, θ_r, causes an increase in the distance between the centroid of the column and the point of reaction force, d_c. From Eqs.(11.a,c), both M_A and M_N increase in accordance with the increment in d_c. As a result, rotational stiffness of the column base with SMA anchorage did not always decrease, even when yielding apparently occurred in the SMA anchor bolts.

NUMERICAL SIMULATION OF EXPOSED-TYPE COLUMN BASE WITH SMA ANCHORAGE

Based on these experimental results, the following assumptions were made in the numerical model of the column base with SMA anchorage.

1) Point of reaction force can be determined from the axial force and rotation of the base plate.
2) Clearance between the base and base plate is linearly proportional to the distance from the point of reaction force.
3) Degradation of the rotational stiffness of the column base due to elastic deformation can be estimated by using a rotational stiffness modification coefficient [8].

Distance between the centroid of the column and the reaction force, d_c, is a function θ_r and N:

$$d_c = f(\theta_r, N) \tag{12}$$

and can be expressed as a bi-linear line shown in Fig. 14.

The anchor bolt consists of two different sections (SMA rod and steel bolt), and is tight against base plate, and thus there is no looseness between the anchor bolt and base plate. The following compatibility condition is therefore satisfied during loading:

$$\delta_A + \delta_B = (d_c + d_t)\cdot\theta_r \tag{13}$$

where δ_A is elongation of the tensile-side anchor bolt and δ_B is vertical displacement due to elastic deformation of the base and base plate as follows.

$$\delta_A = \varepsilon\cdot\ell_b + \frac{P\cdot\ell_s}{n\cdot E_s\cdot A_s}, \quad P = n\cdot\sigma\cdot A_b$$

$$\delta_B = (R-1)\cdot\left(\frac{P\cdot\ell_s}{n\cdot E_s\cdot A_s} + \frac{P\cdot\ell_b}{n\cdot E_b\cdot A_b}\right) \tag{14.a,b,c}$$

σ, ε, n : Stress, strain, and number of tensile-side anchor bolt
E_b, A_b, l_b : Young's modulus, sectional area, and length of SMA rod
E_s, A_s, l_s : Young's modulus, sectional area, and length of typical steel bolt
P : Tensile force of tensile-side anchor bolt
R : Rotational stiffness modification coefficient

The σ vs. ε relation of the SMA rod given by Eqs.(1-4) can be summarized as follows.

$$\varepsilon = g(\sigma, T_a) \tag{15}$$

When N and T_a are given, a set of (σ, ε, θ_r) can be solved by using Eqs.(12)-(15), and then M, Q, and δ_h are derived as follows.

$$M = (d_c + d_t)\cdot P - d_c\cdot N$$

$$Q = M / L$$

$$\delta_h = \frac{M\cdot L^2}{3\cdot E\cdot I_c} + \theta_r\cdot L \tag{16.a,b,c}$$

Simulation results

The simulated M vs. θ_r relation was determined for four different types of SMA anchorage in an exposed-column base as summarized in Table 4.

Case 1: Same material (A) and cross-section of SMA rod used as specimen in loading test.

Case 2: Material of the SMA was material B (Table 1).
Other conditions were the same as Case 1.

Case 3: Cross-sectional area of SMA rod was 3.3 times that for Case 2.
Other conditions were the same as Case 2.

Case 4: Length of SMA rod was half that for Case 3.
Other conditions were the same as that for Case 3.

The loading program was cyclic loading with incremental intensity and incremental amplitude from θ_r =0.010 rad to θ_r =0.040 rad in increments of 0.005 rad, and N = 196 kN and T_a = 295 K (22^{o}C).

Figure 3 shows M vs. θ_r for each of the four cases. The results can be summarized as follows.

1) An SMA rod of appropriate material and dimensions yields a M vs. θ_r relation that has a spindle-shaped hysteresis loop, indicating that this rod can absorb energy effectively.
2) Resistance characteristics and the initial elastic limit rotation and strength can be adjusted by changing the cross-sectional area and length of the SMA rod and steel bolt.
3) Excessive deformation of column base beyond a certain limit can be avoided because the rotational stiffness in M vs. θ_r relation drastically increases from a certain rotation of base plate.

Table 4: Material properties and dimensions of different SMA anchorage in numerical model of column base.

	A_b	l_b	E_b	A_s	l_s	E_s	SMA
	mm^2	mm	GPa	mm^2	mm	GPa	Material Properties
Case1	78.5	225	40	573	497	205.8	A
Case2	78.5	225	29	573	497	205.8	B
Case3	257.4	225	29	573	497	205.8	B
Case4	257.4	112.5	29	573	609.5	205.8	B

E_c =205.8 (GPa), I_c =4.98x10 (mm^4), d_t =150 (mm) , L =910 (mm), R =1.6, n =2

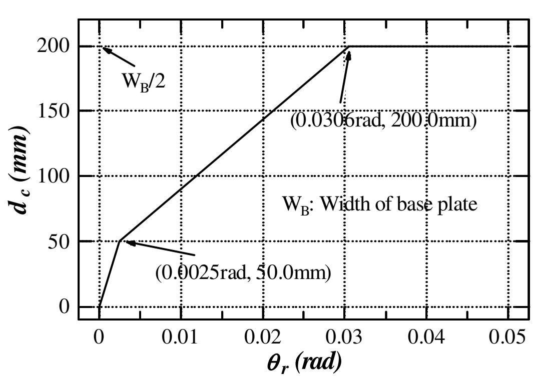

Figure 14: Assumed d_c vs. θ_r relation.

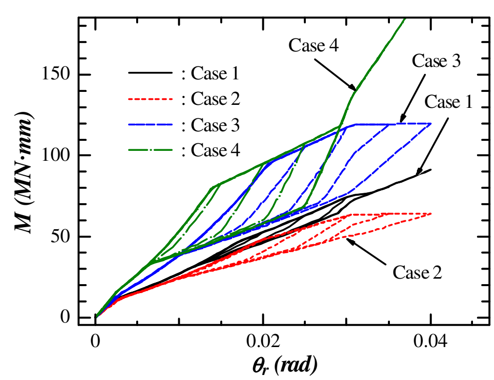

Figure 15: Analytical M vs. θ_r for column base with SMA anchorage

CONCLUDING REMARKS

We developed an application of SMA rod as a seismic-resistant member in an exposed-type column base of building structures. To clarify the resistance mechanism of a column base with SMA anchorage, pulsating loading tests were done using cantilevers with SMA anchorage and typical anchorage. After a numerical model of a column base with SMA anchorage was derived, simulations under cyclic loading were performed. Both the experimental and simulation results demonstrate the applicability and availability of SMA rods for building column bases.

Conclusions from experimental results about the fundamental mechanism of the column base are as follows.

1) The bending moment at the end of a column can be separated into components of axial force and tensile force of the anchor bolts.

2) With increasing rotational angle of the base plate, the point of concentrated reaction force becomes further from the centroid of the column.

3) Due to the elastic deformation of the base plate and steel base, rotational stiffness of the column base is considerably smaller than that when the base plate and steel base are assumed to be rigid.

4) Leverage of the base plate causes the anchor bolt to bend when the rotational angle is relatively large ($\delta_h > 5\delta_y$).

Conclusions from both experimental and simulation results about the resistance and deformation characteristics of a column base with SMA anchorage and that with typical anchorage are as follows.

1) The relation between the bending moment at the end of the column and the rotational angle of the base plate is slip type for typical anchorage, and spindle-shaped hysteresis for SMA anchorage.

2) For typical anchorage, the residual deformation accumulates in accordance with the number of loading cycles. The anchor bolt comes out from the base, and therefore, there is no restoring force in the column base. On the contrary, the SMA anchor bolts recover their original shape and their resistance performance after repeated large rotations of the base plate. Large restoring force can be expected in the column base with SMA anchorage.

3) Due to leverage of the base plate, the deformation capacity of SMA anchorage is less than that under a pulsating tension loading test [6]. Furthermore, the notch of the screw joint in the SMA rod causes brittle fracture.

Conclusions from the numerical simulation on the column base with SMA anchorage are as follows.

1) The initial elastic limit displacement and strength are adjustable by changing the length and cross-sectional area of the steel bolt and the cross-sectional area of the SMA rod.

2) Restoring force characteristics do not degrade and the seismic energy inputted to the structural frame is absorbed effectively due to the pseudoelastic deformation of the SMA rod.

In conclusion, SMA anchorage can improve the restoring force characteristics of a column base and can prevent plastic deformation and damage in the column. Furthermore, it is possible to design a column base with SMA anchorage that does not require repair after a severe earthquake, when the maximum rotation responses of the base plate are less than 0.025 rad.

To develop a column base with SMA anchorage that has improved performance, SMA must be developed that has larger energy absorption capacity and ductility. Further material development is expected, due to the demand for smart structural systems.

ACKNOWLEDGMENTS

This research was done as part of a SMA working group under the US-Japan Cooperative Structural Research Project on Smart Structural Systems (Chairperson, Prof. S. Otani, University of Tokyo; and Chairperson of Subcommittee on Effector Technology, Prof. T. Fujita, Univ. of Tokyo). We would like to acknowledge Dr. T. Takamatsu from Hiroshima Institute of Technology, for the use of the loading systems (Facilities in Hiroshima Institute of Technology, Private School Grant-in-Aid from Ministry of Education, Science and Culture of Japan). Also, we thank Dr. Y. Shugo from Daido Steel Co. Ltd., and Mrs. M. Takeshita, K. Ishihara and S. Sugimoto from Hiroshima Univ., for their cooperation in doing the experiments. This work was supported by a Grant-in-Aid from the Ministry of Education, Science and Culture of Japan（Prof. Y. Kitagawa, Fundamental Study on Smart Structural System for Building, No.13450227）

REFERENCES

1. K.Tanaka.(1986):"A thermo mechanical sketch of shape memory effect; one-dimensional tensile behavior ",*Res.Mech.*,Vol.18,pp.19-33.
2. E.J.Graesser, F.A.Cozzarelli,(1991):"Shape-memory alloys as new materials for aseismic isolation", *Journal of engineering mechanics*, Vol.117-11,pp.2590-2608.
3. W.Huang (2000):"Modified shape memory alloy(SMA) model for SMA wire based actuator design", *J.Intell. Mater. Syst. Struct.*,, Vol.10, pp.221-231.
4. R.DesRoches, R.Leon, G.Hess(2001):"Seismic design and retrofit using shape memory alloys", *Earthquake engineering frontiers in the new millennium*, Swts & Zeirlinger, pp.419-424.
5. H.Tamai.,K.Kondoh,, M.Hanai,(1999):"On mechanism of X-braced frame with hysteretic damper and its elasto-plastic behavior", *J. Struct. Constr. Eng., AIJ* , Vol.515, pp.139-146 (in Japanese).
6. H.Tamai,Y.Kitagawa(2002),"Pseudoelastic behavior of shape memory alloy wire and its application to seismic resistance member for building", *Computational materials science*, 25, pp.218-227.
7. S.Sugimoto, M.Takeshita, H.Tamai, Y.Kitagawa et al. (2003),"Smart structure system using pseudo elasticity of shape memory alloy – Application to anchor bolt for column base and its mechanical characteristics- ", *11th Japanese symposium on earthquake engineering*, pp.1935-1940 (in Japanese).
8. AIJ(1990), Recommendation for design of steel tube structures, pp.127-128 (in Japanese).